Microchimica Acta (2022) 189:415
https://doi.org/10.1007/s00604-022-05509-w

ORIGINAL PAPER

Paper-based device for the selective determination of doxycycline antibiotic based on the turn-on fluorescence of bovine serum albumin–coated copper nanoclusters

Yiming Bu[1] · Ranhao Yin[1] · Long Yu[1] · Pengchen Su[1] · Zibiao Li[2,3] · Enyi Ye[2,3] · Xian Jun Loh[2] · Houjuan Zhu[2] · Suhua Wang[1]

Received: 2 August 2022 / Accepted: 21 September 2022 / Published online: 11 October 2022

Abstract

An enhanced ratiometric fluorescence sensor was built for on-site visual detection of doxycycline (DOX) through the interaction with bovine serum albumin on the surface of red emissive copper nanoclusters. Upon the addition of weakly fluorescent DOX, the red fluorescence from copper nanoclusters gradually decreased through the inner-filter effect (IFE), while a green fluorescence appears and significantly increases, forming an interesting fluorescent isosbestic point, which was assigned to DOX due to sensitization effect of bovine serum albumin. On the basis of this ratiometric fluorescence, the system possessed good limit of detection (LOD) of 45 nM and excellent selectivity for DOX over other tetracyclines. Based on these findings, a paper-based sensor has been fabricated for distinct visual detection of trace DOX and combined with smartphone color recognizer for quantitative detection of DOX (LOD = 83 nM). This method shows broad application prospects in environmental monitoring and food safety.

Keywords Copper nanoclusters · Doxycycline detection · Structural recognition · Ratiometric fluorescence detection · Inner filter effect

Introduction

Doxycycline (DOX), a semisynthetic tetracycline antibiotic, has been extensively applied in animal husbandry and aquaculture because of its low price and high effectiveness [1]. However, it is difficult to degrade DOX in the short term and the consequent DOX residues are easily accumulated in common human foods, including milk, drinking water, vegetables, and eggs. Long-term consumption of food containing DOX may cause serious diseases, such as hepatotoxicity and gastrointestinal disorder [2]. Therefore, it is of great significance to develop an effective method to detect DOX residues in food. So far, many techniques for detecting DOX have been developed, including HPLC [3], HPLC–MS/MS [4], UPLC [5], electrochemical methods [6], colorimetry [7], surface plasma resonance [8], and fluorescence analysis. However, most of these methods with high sensitivity can only be conducted in well-equipped laboratories due to their demand of complex sample preparation procedures, expensive instruments, time-consuming pretreatment process, and professional technicians. Thus, it is important to develop a rapid, simple, and selective method for detection of DOX.

Fluorescence analysis is one of the most popular analytical methods at present. It has the advantages of fast analysis speed, high sensitivity, good selectivity, and simple operation, which has aroused the interest of many researchers. It is noteworthy, however, that most of the fluorescence probes rely on single emission fluorescence signal and have some defects. Compared with single emission fluorescence probe, the ratiometric fluorescence probe has the characteristics of

✉ Houjuan Zhu
zhu_houjuan@imre.a-star.edu.sg

✉ Suhua Wang
wangsh@gdupt.edu.cn

1 Guangdong Provincial Key Laboratory of Petrochemical Pollution Processes and Control, School of Environmental Science and Engineering, Guangdong University of Petrochemical Technology, Maoming 525000, People's Republic of China

2 Institute of Materials Research and Engineering, A*STAR (Agency for Science, Technology and Research), Singapore 138634, Singapore

3 Institute of Sustainability for Chemicals, Energy and Environment (ISCE2), A*STAR (Agency for Science, Technology and Research), Singapore 138634, Singapore

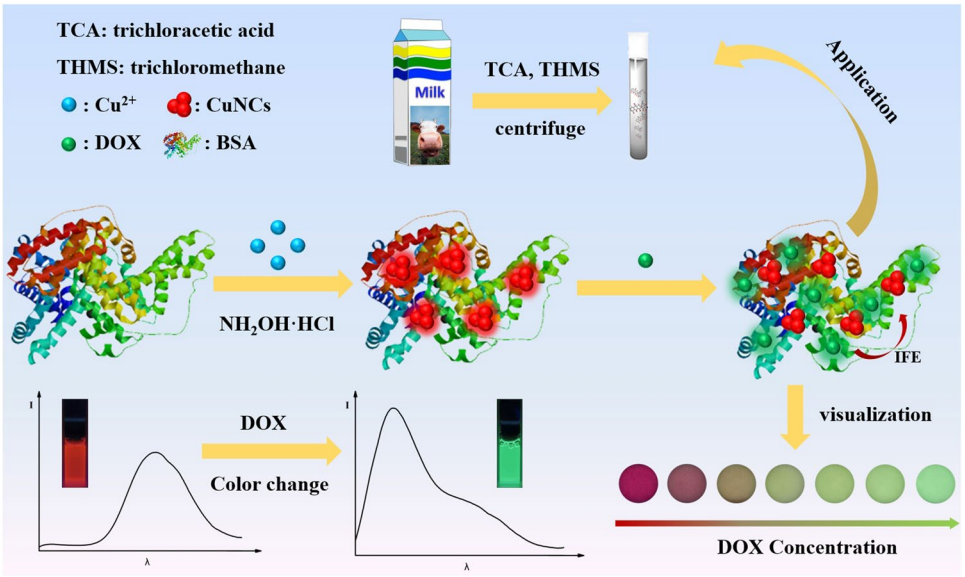

Scheme 1 Synthesis schematic diagram of CuNCs@BSA and the fluorescence response to DOX

dual emission fluorescence and the self-calibrating function of correction signal, which can reduce the detection error caused by various environmental factors [9, 10]. In recent years, a few ratiometric fluorescence sensors were developed for the detection of DOX. For example, Tang et al. developed a ratiometric fluorescence probe based on co-doped graphene quantum dots and rhodamine B for detection of doxycycline [11]. Zhuang et al. reported a ratiometric fluorescent probe that was designed based on sulfur quantum dots and Ca^{2+} [12]. However, due to the existence of multiple fluorophores, the preparation of ratiometric fluorescence probe becomes complicated. Ding et al. established a ratiometric probe to detect DOX based on gold nanoclusters [13]. Currently, an increasing number of ratiometric fluorescence sensors have been designed for detection, in which there are usually two or more fluorophores such as rare-earth ions (Eu^{3+}), carbon dots, and dyes assembled together by chelation to form complexes [14, 15]. However, the preparation of ratiometric fluorescence probe becomes complicated due to the existence of multiple fluorophores and the synthetic raw materials of nanomaterials paid a high price. Therefore, it is still an unmet challenge to develop a facile and rapid sensor for determination of DOX until now.

Copper nanoclusters (CuNCs), a kind of novel fluorescence nanomaterials, have been extensively used in the field of fluorescence sensing because of the ultra-fine size, good biocompatibility, low toxicity, and large Stokes shift [16]. Compared with gold and silver nanoclusters, they also have abundant source and low cost [17, 18]. However, the surface of nano-sized copper nanoclusters is easy to be oxidized, resulting in poor dispersion. Thus, it is difficult to prepare copper nanoclusters with high stability. Up to day, there are few reports about them. In recent years, copper nanoclusters using bovine serum albumin (BSA) as stabilizer have been widely reported because of their good stability, strong oxidation resistance, and high fluorescence signal [19]. Wang et al. prepared red-emitting copper nanoclusters as a reducing agent for detection of rutin. Aparna et al. developed a sensor to detect both protamine and heparin sensitively and selectively [20]. Garima et al. synthesized a fluorescent nanoprobe for ratiometric detection of hydroxyl radicals and superoxide anion radicals [21]. Particularly, the interaction mechanism between BSA and copper nanoclusters are also studied to facilitate understand BSA stabilized CuNCs and expand their better application in biological applications [22, 23]. Therefore, the fluorescence strategy constructed by BSA-stabilized fluorescent copper nanoclusters has better analytical performance [24, 25]. It has been reported that there are many hydrophobic binding cavities in the three-dimensional structure of BSA, which can combine with DOX, leading to the increased quantum yields (QYs) of DOX [26, 27]. Therefore, the fluorescence of DOX can be sensitive to BSA.

Herein, this work reports a novel ratiometric system for visual detection of DOX based on the interaction between BSA-stabilized copper nanoclusters (CuNCs@BSA) and DOX (Scheme 1). The prepared CuNCs@BSA shows excellent fluorescence performance with a QY of 11.25%. Upon adding the DOX, the red fluorescence of CuNCs is quenched via the inner filter effect (IFE) and the green fluorescence of DOX is enhanced by sensitization effect of BSA on DOX. The CuNCs@BSA possess good water solubility and high stability, and their starting raw materials are cheap and widely available. The synthetic procedure was carried out under room-temperature conditions with a simple and convenient method. Based on these findings, the probe CuNCs@BSA is further designed as a paper-based sensor

for the visual detection of DOX and applied for the determination of DOX in milk samples.

Experimental section

Chemicals and materials

Copper nitrate trihydrate ($Cu(NO_3)_2{\cdot}3H_2O$), bovine serum albumin (BSA), hydroxylamine hydrochloride ($NH_2OH{\cdot}HCl$), sodium hydroxide (NaOH), hydrochloric acid (HCl), trimethylol aminomethane (Tris), doxycycline (DOX), tetracycline (TC), oxytetracycline (OTC), chlortetracycline (CTC), chloramphenicol (CHL), kanamycin (KAN), ceftriaxone sodium (CEF), streptomycin (STR), and ampicillin (AMP) were purchased from Aladdin Reagents Co. Ltd. (Shanghai, China). Inorganic salts (KCl, $CaCl_2$, NaCl, $MgSO_4$, $AlCl_3$, $ZnSO_4$), histidine (His), serine (Ser), phenylalanine (Phe), lysine (Lys), glycine (Gly), and cysteine (Cys) were supplied by Macklin Co. Ltd. (Shanghai, China). All the chemicals and solvents were of analytical reagent grade without any treatment. Ultrapure water (18.25 MΩ·cm; Millipore Co., USA) was used for the preparation of all aqueous solutions.

Preparation of BSA-stabilized Cu nanoclusters and fluorescent quantum yield measurement

BSA-stabilized Cu nanoclusters (CuNCs@BSA) were synthesized according to a reported procedure with minor modification [28]. Detailed synthesis steps are described in the Electronic supporting material (ESM). The *QY* of CuNCs@BSA was tested by single-point measurement using rhodamine 6G (*QY* = 0.95 in EtOH) as standard:

$$\mathrm{QY}(\%) = \mathrm{QYq}\frac{I_s A_q (\eta_s)^2}{I_q A_s (\eta_q)^2}$$

where *I* is the fluorescent emission intensity, *A* is the absorbance, and η is the refractive index of the solvent. The subscripts q and s signify fluorescent standard samples and experimental samples, respectively.

Detection of doxycycline and preparation of paper sensor

To optimize the detection conditions, 100 µL aqueous solution of CuNCs@BSA was added into a quartz fluorescence cuvette. DOX solutions of different concentrations were successively added into the detection system. Then, the system was diluted to 2.0 mL with Tris–HCl buffer solution. The final concentration of CuNCs@BSA was 5 mg mL^{-1}. After incubating at room temperature for 1 min, the fluorescence spectra of the samples were determined in the range from 470 to 850 nm under excitation wavelengths of 365 nm with a filter of 450 nm. To validate this approach for practical application, other antibiotics, amino acids, and cations were used for the selective measurements. All experiments were performed three times. Error bars represent the standard deviations of measurements with triplicate trials (σ is the standard deviation of the blank and *m* is the slope of the calibration plot).

For the visual detection of DOX, the paper-based sensor was fabricated by loading the CuNCs@BSA ratiometric probe on Whatman glass microfiber filter paper. Briefly, a series of 15 µL of the CuNCs@BSA (20 mg mL^{-1}, pH = 7.5) solution was dropped onto a piece of filter paper (0.6 mm in diameter). Then, 15 µL of different concentrations of DOX aqueous solution were carefully dropped onto the center of a circular filter paper and air-dried under ambient condition. The color of the test paper was observed under 365 nm UV lamp and recognized by a color recognizer APP in the smartphone.

Fluorescence assay of doxycycline in milk

In order to reduce the interference of fluorescence detection, 3 mL of milk samples was first diluted with 6 mL of ultrapure water. Since protein and fat in milk may affect the determination of tetracyclines, 2 mL of 10% trichloroacetic acid and trichloromethane was added into the centrifuge tube of the diluted milk samples followed by vortexing for 90 s and ultrasonicating for 20 min. Then, the mixture was centrifuged twice at 10,000 rpm for 15 min. The obtained supernatant was used for the detection of DOX.

Characterization

Fluorescence spectra were recorded using a F-7100 fluorescence spectrophotometer (Tokyo, Japan) equipped with 1-cm quartz cuvettes and an analysis unit. UV–Vis absorption spectra were determined by a UV–Vis 2600i spectrophotometer (Tokyo, Japan). Fourier-transform infrared (FTIR) spectra were measured by a Thermo Fisher Nicolet iS10 Fourier Transform infrared spectrometer. The X-ray diffraction (XRD) spectrum analysis was performed using a Shimadzu XRD-600 diffractometer (Kyoto, Japan). Morphology and size distribution of prepared samples were obtained by Tecnai G2 F20 transmission electron microscope (FEI, USA). X-Ray photoelectron spectroscopy (XPS) was measured by VG Multilab 2000X high-performance electron spectrometer (Thermal Electron, USA). Zeta potential and dynamic light scattering (DLS) were tested on a Zetasizer Nano Series analysis meter (ZS 90).

Interaction of BSA with doxycycline

The interaction between BSA and DOX was evaluated with the fluorometric method [29]. Two milliliters of BSA (50 μM) was added into a quartz fluorescence cuvette and then titrated by successive additions of DOX (1.0 mM) to obtain a series of final concentrations. Fluorescence spectra were recorded in the range of 300–500 nm. The double-logarithmic equation was used for analyzing the fluorescence data:

$$\lg\left[\left(F_0 - F\right)/F\right] = \lg K_b + n \lg[Q]$$

where F_0 and F are respectively the fluorescence intensities of the fluorophore before and after adding the quencher; K_b and n respectively refer to the binding constant and binding-site number.

Results and discussion

Characterization of BSA-stabilized Cu nanoclusters

The structure and morphology of the synthesized CuNCs@BSA were characterized by high-power transmission electron microscopy (HRTEM). As depicted in Fig. 1a and c, CuNCs@BSA is monodispersed spherical with the particle sizes in the range of 8–12 nm. The lattice spacing of 0.21 nm shown in Fig. 1b is consistent with the (111) planes of the metallic Cu [30], indicating that CuNCs@BSA has been successfully prepared. Then, the size distribution of CuNCs@BSA in aqueous solution is further measured by the measurement of dynamic light scattering (DLS) (Fig. S1). The result indicates that the average hydrodynamic diameter size of CuNCs@BSA is about 16.1 nm, which is larger than the size measured from HRTEM due to macromolecule BSA coating layer on the surface of CuNCs. The formation of such ultrasmall and uniform NCs is mainly due to the strong multichelating effects from BSA that can control the growth of NCs.

To explore the crystalline structure of CuNCs@BSA, the X-ray diffraction (XRD) spectrum was determined. As depicted in Fig. 2a, the XRD peaks are generally widened, suggesting a less crystalline structure. Also, the broader diffraction peak (2θ) at 43.2° with index of (111) is found in the latter, which is consistent with the standard data on a JCPDS card (no. 65–6801), implying the existence of Cu^0 [31]. The diffraction peak located at 20.8° may be ascribed to amorphous structure of CuNCs@BSA and surface coating of BSA. Beyond this, the zeta potential of CuNCs@BSA in aqueous solution was measured to be – 32.9 mV (Fig. S2), indicating that the negatively charged BSA stabilizer is decorated on the surface of the CuNCs [32]. The ingredients and chemical states of element in CuNCs@BSA were analyzed by XPS spectrum. Survey spectrum (Fig. 2b) of CuNCs@BSA indicates the presence of Cu 2p (0.19%), C 1 s (53.79%), O 1 s (23.10%), N 1 s (21.06%), and S 2p (1.86%). As shown in Fig. 2c, two characteristic peaks of the Cu 2p spectrum at 932.5 eV and 952.6 eV are assigned to Cu 2p 3/2 and Cu 2p 1/2 of Cu, respectively, indicating the presence of Cu (0) and Cu (I) [33]. There is no satellite peak at 942.0 eV, which confirms the absence of Cu (II) in CuNCs@BSA. Moreover, the S_2^{2-} 2p3/2 and S_x^{2-} 2p1/2 peaks can be obviously observed at 162.7 and 163.9 eV in the XPS narrow spectrum of S 2p (Fig. 2d), which are assigned to the bound sulfhydryl of BSA, confirming that BSA is combined

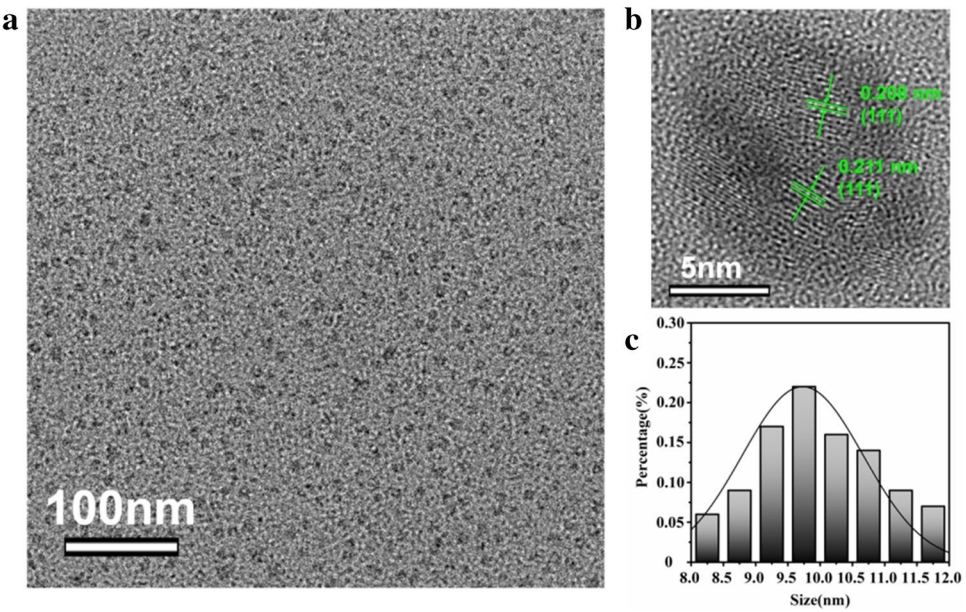

Fig. 1 Structure and size characterization of CuNCs@BSA. **a** HRTEM images of the as-prepared CuNCs@BSA. **b** HRTEM image of the CuNCs@BSA. **c** Size distribution of the CuNCs@BSA through statistical HRTEM images

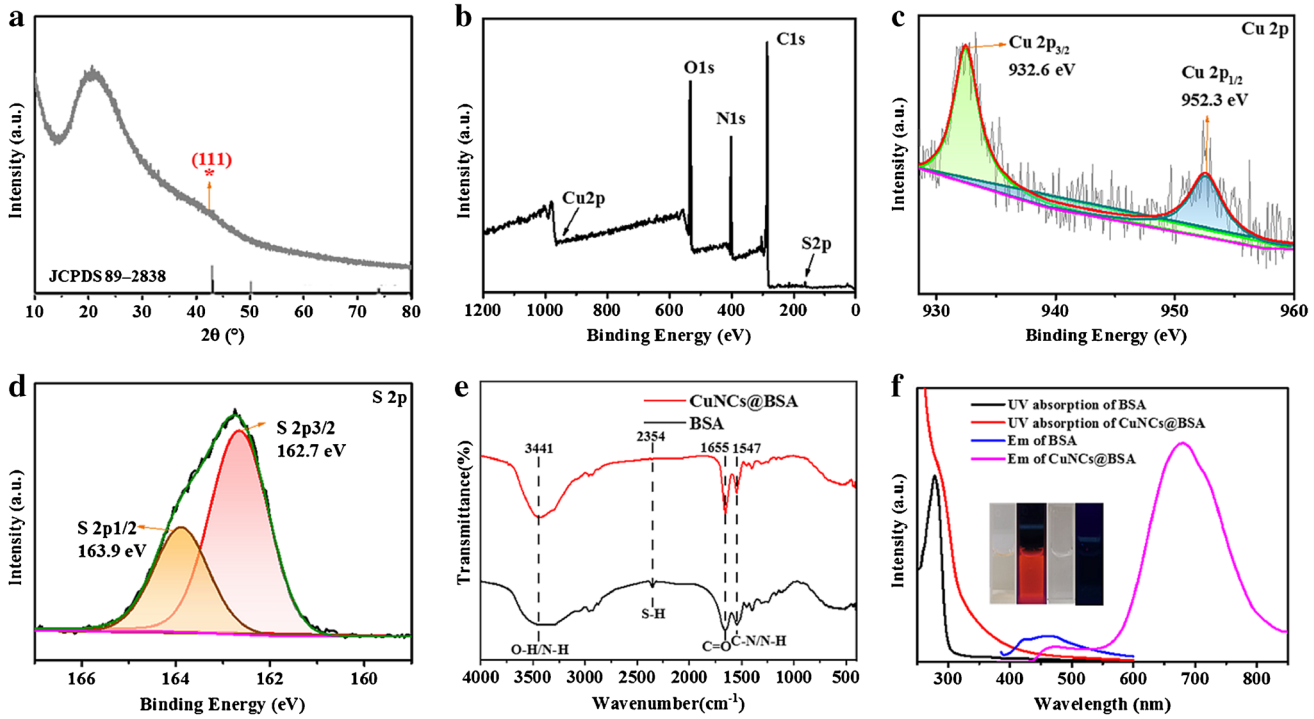

Fig. 2 Spectral characterization for CuNCs@BSA. **a** XRD spectrum of CuNCs@BSA. **b** XPS survey spectrum of CuNCs@BSA. **c** High-resolution XPS spectrum of Cu 2p. **d** High-resolution XPS spectrum of S 2p. **e** FT-IR spectrum of CuNCs@BSA and BSA. **f** UV–Vis absorption and fluorescence emission spectra of CuNCs@BSA and BSA (inset: photographs of the CuNCs@BSA and BSA dispersion taken under sunlight and 365-nm UV lamp)

with CuNCs through the Cu–S bond [34–36]. To further study the surface groups and component of CuNCs@BSA, FTIR was used for characterization (Fig. 2e). The peak at 1655 cm^{-1} corresponds to the stretching vibrations of C = O; the peak at 1547 cm^{-1} was ascribed to C–N stretching and N–H bending vibration. The peaks centered within the range of 3000–3500 cm^{-1} confirm the presence of O–H and N–H bonds [37]. In addition, in comparison with FTIR of BSA, the peak at 2352 cm^{-1} assigned to the stretching vibrations of S–H bond disappeared after synthesis of CuNCs@BSA [38]. Such phenomenon may be attributed to the interaction between the sulfhydryl group in the BSA and Cu. Consequently, this result further implies the successful formation of CuNCs@BSA.

The UV–Vis absorption spectra (Fig. 2f) indicate that the CuNCs@BSA had obvious absorption peaks at 280 nm, which are derived from the aromatic amino acids (Trp, Tyr, and Phe) in BSA. Noteworthy, the characteristic surface plasmon resonance peak of CuNCs is not observed about in the range from 500 to 600 nm, indicating the absence of any large copper nanoparticles and the effective formation of CuNCs@BSA [39]. The prepared CuNCs@BSA exhibits superior dispersibility in aqueous solution, and red fluorescence is obviously observed under illumination with a 365-nm UV lamp (inset of Fig. 2f). Their quantum yield (QY) is calculated to be 11.25% in aqueous solution, which is higher than that of many metal nanoclusters. In particular, the light yellow freeze-dried CuNCs@BSA powder is found to still exhibit red fluorescence under UV irradiation (Fig. S3), showing their fluorescence stability. In addition, it is acknowledged that fluorescence stability of probe is a key factor during sensing process. Thus, the fluorescence change of CuNCs@BSA under different conditions is monitored. It is clearly seen from Fig. S4 that the fluorescence intensity of CuNCs@BSA still keeps constant in different solution conditions, including various ionic strengths, temperatures, illumination time, and pH values. Obviously, no fluorescence intensity change is observed when the solution of CuNCs@BSA is irradiated once a day for 1 week (Fig. S5), indicating that CuNCs@BSA has excellent fluorescence stability that facilitated the further detection of DOX.

Detection of doxycycline in fluorescence manners

Before investigating the DOX determination, it is essential to optimize detection parameters (incubation time and solution pH) for improving detection sensitivity of DOX. The response of fluorescence to incubation time was first monitored (Fig. S6A). It can be clearly observed that F_{520}/F_{673} increases rapidly and tends to stabilize after 1 min with the

addition of DOX into probe solution, suggesting that the DOX could efficiently react with CuNCs@BSA in a short time. Therefore, the best detection time is fixed to be 1 min after adding DOX. Simultaneously, the influence of pH values on DOX detection is also investigated. As depicted in Fig. S6B, the fluorescence response of ratiometric system to DOX shows a slight variation in the pH range from 5 to 9. In detail, such response increases below pH 7.5 and decreases with the increase in pH values. This phenomenon may be on account for the destruction of BSA structure at both very low and high pH conditions, inducing the interaction between CuNCs@BSA and DOX, conclusively influencing their inner filter effect (IFE) and sensitization effect. Thus, these results show that the ratiometric maximum response toward DOX occurred at pH 7.5. Accordingly, pH 7.5 is applied in further tests.

Under the optimized conditions, the analytical performance of the fluorescence sensing method is researched. With the increase of DOX concentration, the fluorescence intensity of CuNCs@BSA decreases at 673 nm, while a new peak appears at 520 nm (Fig. 3a). It is interesting that a fluorescence isosbestic point was found at around 625 nm as fluorescence quenches and turns on at 673 nm and at 520 nm, respectively. The corresponding fluorescence color changes from red to green under the irradiation of a 365-nm UV lamp (inset of Fig. 3b). In addition, there exhibits a good linear relationship between CuNCs@BSA probe and the concentration of DOX. As shown in Fig. 3b, a linear relation between F_{520}/F_{673} and DOX concentration is observed in the range of 0–30 μM with a correlation coefficient of $R^2 = 0.996$, and the corresponding limit of detection (LOD) is 45 nM ($3\sigma/m$, where σ is the standard deviation of blank solution and m is the slope of the calibration plot). When compared with the reported results in Tab. S1, CuNCs@BSA possesses simpler synthesis, cheaper raw material, and lower LOD than that of reported ratiometric fluorescent probes for DOX. Besides this, the distinguishment of DOX from other tetracycline antibiotics is also achieved by the sensor. Also, the CuNCs@BSA-based sensor platform combined with smartphone application realizes the portable, visual, and quantitative monitoring of DOX.

Selectivity and interfering factors are key indexes to evaluate the detection performance of fluorescent probes. In this study, some metal cations (K^+, Ca^{2+}, Na^+, Mg^{2+}, Al^{3+}, Zn^{2+}), amino acids (His, Cys, Phe, Ser, Lys, Gly), and antibiotics (AMP, STR, CEF, CHL, KAN) are selected as interference ions to verify the selectivity and interfering factors of CuNCs@BSA composite system in DOX detection. As shown in Fig. 3c and d, the response value of the ratiometric fluorescent probe changes significantly in the presence of DOX. However, for other interfering analytes, even when the concentration is much higher than DOX, the response value of the ratiometric fluorescent probe only shows slight changes.

The responses of CuNCs@BSA probe toward other tetracycline antibiotics are also carefully studied due to their highly similar structure (Fig. S7). As shown in Fig. S7A, the characteristic fluorescence emission peak at 520 nm is

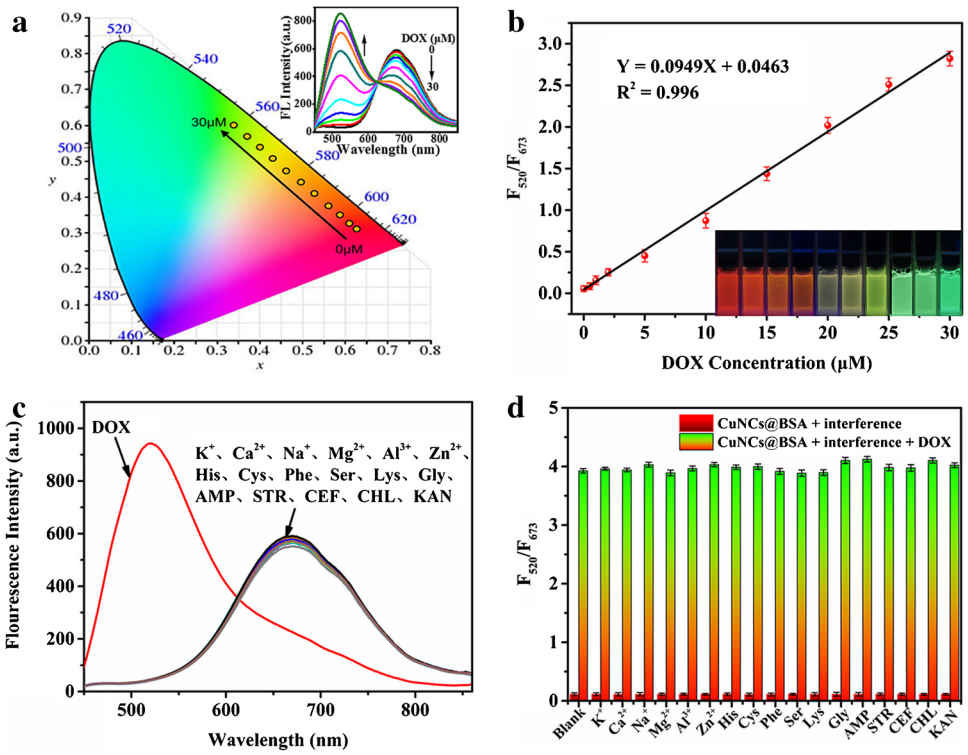

Fig. 3 Ratiometric DOX determination by CuNCs@BSA dispersions. **a** CIE chromaticity diagram of CuNCs@BSA after adding different concentrations of DOX with excitation at 365 nm. Inset: emission spectra of CuNCs@BSA with increasing concentrations of DOX. **b** The linear relationships between F_{520}/F_{673} and the concentration of DOX ($\lambda_{ex} = 365$ nm). The data are presented as the mean ± SD, $n = 3$. Inset: the visualization fluorescent photographs were taken under illumination by a 365-nm UV lamp. **c** Fluorescence responses of the ratiometric probe to different kinds of cations, anions, amino acids, and antibiotics. **d** Selectivity and anti-interference of the CuNCs@BSA toward different kinds of cations, anions, amino acids, and antibiotics (DOX, 30 μM; interference: 150 μM). The data are presented as the mean ± SD, $n = 3$

obtained under the assistance of CuNCs@BSA, while other NCs show weak fluorescence or no fluorescence. This phenomenon may be caused by the lower sensitization effect of BSA on them, which can enhance the possibility of the discrimination toward DOX (Fig. S7B).

Detection mechanism for doxycycline

The mechanism of CuNCs@BSA's response to DOX is investigated. As shown in Fig. 4b, a new fluorescence emission band at 520 nm appears after adding DOX, indicating the sensitization effect of BSA on DOX. According to the previous report, there exhibits several hydrophobic binding cavities in the three-dimensional structure of BSA [27]. DOX can combine with the hydrophobic binding cavities of BSA, and the fluorescence intensity of DOX increases under the hydrophobic environment [26]. This phenomenon can be explained by binding-site number (n). According to the double-logarithmic equation of BSA quenched by DOX (Fig. S8), the binding-site number (n) of BSA with DOX is estimated to be nearly 1, showing that DOX can easily enter one of the hydrophobic binding cavities of BSA. The fluorescence emission spectra of DOX in the presence and absence of BSA is shown in Fig. S9. DOX displays a stronger emission band at 520 nm after adding the BSA, further indicating the sensitization effect of BSA. As seen from Fig. 4a, the spectral overlap is discovered among UV–Vis absorption band of DOX and excitation band of CuNCs@BSA. DOX shows strong absorption bands at 365 nm, indicating that the mechanism of fluorescence quenching for DOX might be inner filter effect (IFE) [33].

Paper sensor for doxycycline visual detection

In order to develop a convenient, real-time, and visual detection device for DOX, a paper-based sensor is fabricated (Fig. 5). Different concentrations of DOX aqueous solution were dropped onto the fluorescent paper-based sensor coated with CuNCs@BSA. Under the irradiation of ultraviolet lamp, it can be observed that the color of the test paper changes significantly from red to green with the increase of DOX concentration. The color change is consistent with the change of the reaction in aqueous solution, indicating the successful preparation of fluorescence paper-based sensor for the visual detection of DOX. For improving the accuracy and reliability of the results, RGB analysis of fluorescent images is applied through a Color Recognizer APP (Fig. S10) on a smartphone, which can convert color pictures to RGB values for color identification of DOX. After capturing a series of fluorescence images, DOX concentration is assessed by calculating the ratio of green and red channels. The results show that the ratio of green channel to red channel (G/R) has a good linear relationship with DOX concentration ($R^2 = 0.949$, LOD = 83 nM). The results indicate that the sensor platform combined with smartphone application realizes the portable, visual, and quantitative monitoring of DOX.

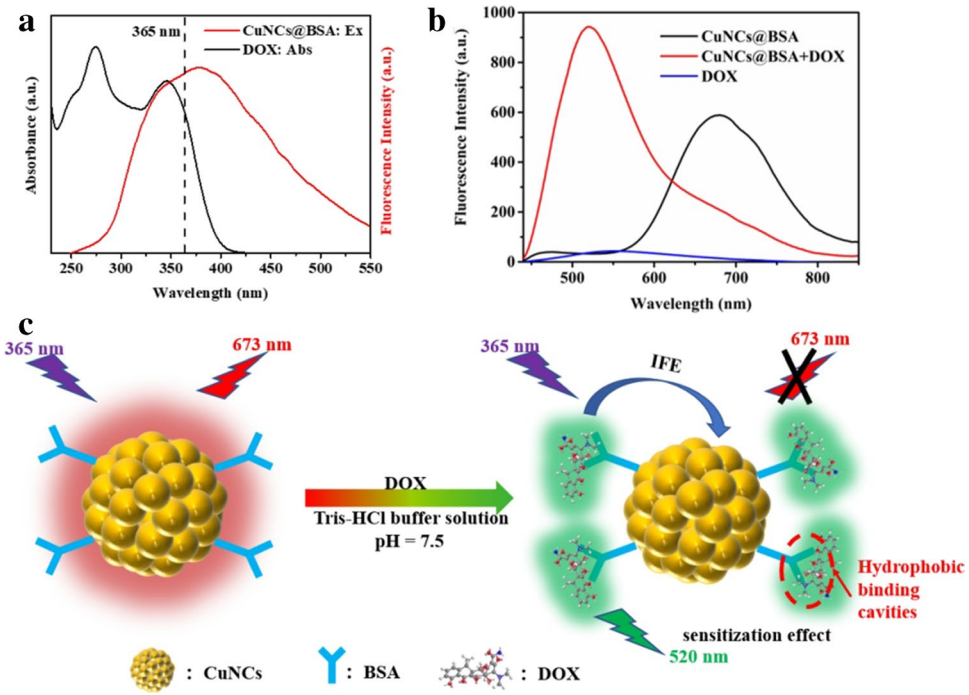

Fig. 4 Proposed DOX detection mechanism by CuNCs@BSA. **a** The UV–Vis absorption spectrum of DOX and fluorescence spectrum of CuNCs@BSA. **b** Fluorescence emission spectra of CuNCs@BSA before and after adding DOX (30 μM) with excitation at 365 nm. **c** Schematic illustration for mechanism of ratiometric detection to DOX by CuNCs@BSA

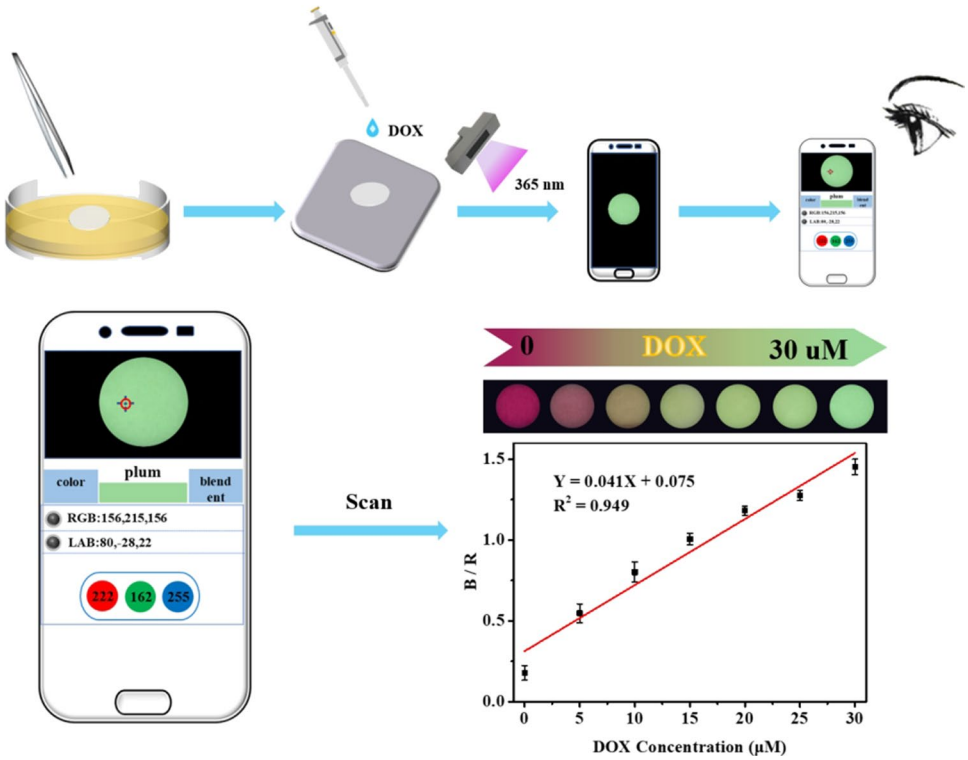

Fig. 5 Schematic drawing for the preparation of test paper sensor and detection of DOX using a smartphone color recognizer. The data are presented as the mean ± SD, $n = 3$

Table 1 Recoveries of the CuNCs@BSA sensor for DOX detection

Spiked concentration	Detected DOX (μM)	Recovery (%)	RSD (%) $n = 3$
0	–	–	–
5	4.8	96.4	2.85
10	10.5	105	3.12
20	19.2	95.9	3.54

Detection of doxycycline in milk

DOX residues in animal food can lead to many adverse reactions, so we used the constructed approach for DOX detection in milk samples by standard recovery test. Different concentrations of DOX standard solution were added to the pre-treated milk samples and the recovery test was conducted. As shown in Table 1, the ratiometric fluorescence sensor still has a sensitive response to DOX in the actual sample system. The recovery rates of DOX range from 96.4 to 105% and the relative standard deviation (RSD) is lower than 3.54%, respectively, indicating that CuNCs@BSA ratiometric fluorescence probe can be used to detect DOX in actual samples.

Conclusion

In conclusion, a valid ratiometric fluorescent sensor is fabricated based on the CuNCs@BSA for visual detection of DOX. The synthesized CuNCs@BSA shows excellent fluorescence stabilities, water solubility, and solid-state luminescence. Such ratiometric probe has been successfully applied in visual detection of DOX by using a paper-based sensor, which provides a simple method for qualitative assay of DOX on-site. In addition, the method has been further applied to determine DOX in milk samples with satisfactory recoveries, providing a potential measurement technique for environmental and food safety monitoring applications. However, compared with some big equipment in laboratory, such device for DOX detection shows relatively high detection range, requires pretreatment of milk-related samples, and requires a UV lamp. These may lead to the translation of this paper-based device to future life safety applicability.

Supplementary Information The online version contains supplementary material available at https://doi.org/10.1007/s00604-022-05509-w.

Funding This work was supported by the National Natural Science Foundation of China (U21A20290, 82001957) and the Guangdong Basic and Applied Basic Research Foundation (2022A1515011656).

Declarations

Conflict of interest The authors declare no competing interests.

References

1. Wang J, Cheng R, Wang Y, Sun L, Chen L, Dai X, Pan J, Pan G, Yan Y (2018) Surface-imprinted fluorescence microspheres as ultrasensitive sensor for rapid and effective detection of tetracycline in real biological samples. Sensors Actuators B Chem 263:533–542. https://doi.org/10.1016/j.snb.2018.02.150
2. van Houten CB, Cohen A, Engelhard D, Hays JP, Karlsson R, Moore E, Fernández D, Kreisberg R, Collins LV, de Waal W, de Winter-de Groot KM, Wolfs TFW, Meijers P, Luijk B, Oosterheert JJ, Heijligenberg R, Sankatsing SUC, Bossink AWJ, Stubbs A, Stein M, Reisfeld S, Klein A, Rachmilevitch R, Ashkar J, Braverman I, Kartun V, Chistyakov I, Bamberger E, Srugo I, Odeh M, Schiff E, Dotan Y, Boico O, Navon R, Friedman T, Etshtein L, Paz M, Gottlieb TM, Pri-Or E, Kronenfeld G, Simon E, Oved K, Eden E, Bont LJ (2019) Antibiotic misuse in respiratory tract infections in children and adults–a prospective, multicentre study (TAILORED Treatment). Eur J Clin Microbiol Infect Dis 38(3):505–514. https://doi.org/10.1007/s10096-018-03454-2
3. Shalaby AR, Salama NA, Abou-Raya SH, Emam WH, Mehaya FM (2011) Validation of HPLC method for determination of tetracycline residues in chicken meat and liver. Food Chem 124(4):1660–1666. https://doi.org/10.1016/j.foodchem.2010.07.048
4. Nebot C, Guarddon M, Seco F, Iglesias A, Miranda JM, Franco CM, Cepeda A (2014) Monitoring the presence of residues of tetracyclines in baby food samples by HPLC-MS/MS. Food Control 46:495–501. https://doi.org/10.1016/j.foodcont.2014.05.042
5. Tylova T, Olsovska J, Novak P, Flieger M (2010) High-throughput analysis of tetracycline antibiotics and their epimers in liquid hog manure using ultra performance liquid chromatography with UV detection. Chemosphere 78(4):353–359. https://doi.org/10.1016/j.chemosphere.2009.11.020
6. Zhou L, Li D-J, Gai L, Wang J-P, Li Y-B (2012) Electrochemical aptasensor for the detection of tetracycline with multi-walled carbon nanotubes amplification. Sensors Actuators B Chem 162(1):201–208. https://doi.org/10.1016/j.snb.2011.12.067
7. Ramezani M, Mohammad Danesh N, Lavaee P, Abnous K, Mohammad Taghdisi S (2015) A novel colorimetric triple-helix molecular switch aptasensor for ultrasensitive detection of tetracycline. Biosens Bioelectron 70:181–187. https://doi.org/10.1016/j.bios.2015.03.040
8. Verma R, Gupta BD (2013) Optical fiber sensor for the detection of tetracycline using surface plasmon resonance and molecular imprinting. Analyst 138(23):7254–7263. https://doi.org/10.1039/C3AN01098H
9. Liu W, Wang X, Wang Y, Li J, Shen D, Kang Q, Chen L (2018) Ratiometric fluorescence sensor based on dithiothreitol modified carbon dots-gold nanoclusters for the sensitive detection of mercury ions in water samples. Sensors Actuators B Chem 262:810–817. https://doi.org/10.1016/j.snb.2018.01.222
10. Zhang F, Wang M, Zhang L, Su X (2019) Ratiometric fluorescence system for pH sensing and urea detection based on MoS2 quantum dots and 2, 3-diaminophenazine. Anal Chim Acta 1077:200–207. https://doi.org/10.1016/j.aca.2019.06.001
11. Tang S, Chen D, Li X, Wang C, Li T, Ma J, Guo G, Guo Q (2022) Promising energy transfer system between fuorine and nitrogen Co-doped graphene quantum dots and Rhodamine B for ratiometric and visual detection of doxycycline in food. Food Chem 388:132936. https://doi.org/10.1016/j.foodchem.2022.132936
12. Zhuang Y, Lin B, Yu Y, Wang Y, Zhang L, Cao Y, Guo M (2021) A ratiometric fluorescent probe based on sulfur quantum dots and calcium ion for sensitive and visual detection of doxycycline in food. Food Chem 356:129720. https://doi.org/10.1016/j.foodchem.2021.129720
13. Ding L, Cao Y, Li H, Wang F, Guo D-Y, Yang W, Pan Q (2022) A ratiometric fluorescence-scattering sensor for rapid, sensitive and selective detection of doxycycline in animal foodstuffs. Food Chem 373:131669. https://doi.org/10.1016/j.foodchem.2021.131669
14. Li W, Zhu J, Xie G, Ren Y, Zheng Y-Q (2018) Ratiometric system based on graphene quantum dots and Eu3+ for selective detection of tetracyclines. Anal Chim Acta 1022:131–137. https://doi.org/10.1016/j.aca.2018.03.018
15. Yu H, Du L, Guan L, Zhang K, Li Y, Zhu H, Sun M, Wang S (2017) A ratiometric fluorescent probe based on the pi-stacked graphene oxide and cyanine dye for sensitive detection of bisulfite. Sensors Actuators B Chem 247:823–829. https://doi.org/10.1016/j.snb.2017.03.101
16. Dong W, Sun C, Sun M, Ge H, Asiri AM, Marwani HM, Ni R, Wang S (2020) Fluorescent copper nanoclusters for the iodide-enhanced detection of hypochlorous acid. ACS Appl Nano Mater 3(1):312–318. https://doi.org/10.1021/acsanm.9b01958
17. Tian X, Kong X-J, Zhu Z-M, Chen T-T, Chu X (2015) A new label-free and turn-on strategy for endonuclease detection using a DNA–silver nanocluster probe. Talanta 131:116–120. https://doi.org/10.1016/j.talanta.2014.07.092
18. Fang X, Zhao Q, Cao H, Liu J, Guan M, Kong J (2015) Rapid detection of Cu2+ by a paper-based microfluidic device coated with bovine serum albumin (BSA)–Au nanoclusters. Analyst 140(22):7823–7826. https://doi.org/10.1039/C5AN01016K
19. Wang B, Gui R, Jin H, He W, Wang Z (2018) Red-emitting BSA-stabilized copper nanoclusters acted as a sensitive probe for fluorescence sensing and visual imaging detection of rutin. Talanta 178:1006–1010. https://doi.org/10.1016/j.talanta.2017.08.102
20. Aparna RS, Anjali Devi JS, Anjana RR, Nebu J, George S (2019) Reversible fluorescence modulation of BSA stabilised copper nanoclusters for the selective detection of protamine and heparin. Analyst 144(5):1799–1808. https://doi.org/10.1039/C8AN01703D
21. Garima JS, Garg S, Matai I, Packirisamy G, Sachdev A (2021) Dual-emission copper nanoclusters–based ratiometric fluorescent probe for intracellular detection of hydroxyl and superoxide anion species. Microchim Acta 188(1):13. https://doi.org/10.1007/s00604-020-04683-z
22. Akhuli A, Chakraborty D, Agrawal AK, Sarkar M (2021) Probing the interaction of bovine serum albumin with copper nanoclusters: realization of binding pathway different from protein corona. Langmuir 37(5):1823–1837. https://doi.org/10.1021/acs.langmuir.0c03176
23. Bhunia S, Kumar S, Purkayastha P (2019) Application of photoinduced electron transfer with copper nanoclusters toward finding characteristics of protein pockets. ACS Omega 4(2):2523–2532. https://doi.org/10.1021/acsomega.8b03213
24. Wang H-B, Chen Y, Li Y, Liu Y-M (2016) A sensitive fluorescence sensor for glutathione detection based on MnO2 nanosheets–copper nanoclusters composites. Rsc Adv 6(83):79526–79532. https://doi.org/10.1039/C6RA17850B
25. Wang H-B, Chen Y, Li N, Liu Y-M (2017) A fluorescent glucose bioassay based on the hydrogen peroxide-induced decomposition of a quencher system composed of MnO2 nanosheets and copper nanoclusters. Microchim Acta 184(2):515–523. https://doi.org/10.1007/s00604-016-2045-7
26. Sun Q, Wang W, Chen Z, Yao Y, Zhang W, Duan L, Qian J (2017) A fluorescence turn-on probe for human (bovine) serum albumin based on the hydrolysis of a dioxaborine group promoted by proteins. Chem Commun 53(48):6432–6435. https://doi.org/10.1039/C7CC03587J
27. Ghorai SK, Samanta SK, Mukherjee M, SahaSardar P, Ghosh S (2013) Tuning of "antenna effect" of Eu(III) in ternary systems in aqueous medium through binding with protein. Inorg Chem 52(3):1476–1487. https://doi.org/10.1021/ic302218m

28. Xu J, Han B (2016) Synthesis of protein-directed orange/red-emitting copper nanoclusters via hydroxylamine hydrochloride reduction approach and their applications on Hg2+ sensing. NANO 11(10):1650108. https://doi.org/10.1142/S1793292016501083
29. Chakraborty B, Sengupta C, Pal U, Basu S (2017) Acridone in a biological nanocavity: detailed spectroscopic and docking analyses of probing both the tryptophan residues of bovine serum albumin. New J Chem 41(21):12520–12534. https://doi.org/10.1039/C7NJ02454A
30. Wang C, Yao Y, Song Q (2016) Interfacial synthesis of polyethyleneimine-protected copper nanoclusters: size-dependent tunable photoluminescence, pH sensor and bioimaging. Colloids Surf, B 140:373–381. https://doi.org/10.1016/j.colsurfb.2016.01.001
31. Said K, Qamhieh N, Awwad F, Ayesh AI (2018) Fabrication and characterization of size-selected Cu nanoclusters using a magnetron sputtering source. Sensors Actuators A 277:112–116. https://doi.org/10.1016/j.sna.2018.03.028
32. Zhang Y, Lv M, Gao P, Zhang G, Shi L, Yuan M, Shuang S (2021) The synthesis of high bright silver nanoclusters with aggregation-induced emission for detection of tetracycline. Sensors Actuators B Chem 326:129009. https://doi.org/10.1016/j.snb.2020.129009
33. Zhao C, Jiao Y, Gao Z, Yang Y, Li H (2018) N, S co-doped carbon dots for temperature probe and the detection of tetracycline based on the inner filter effect. J Photochem Photobiol, A 367:137–144. https://doi.org/10.1016/j.jphotochem.2018.08.023
34. Ding L, Zhao Y, Li H, Zhang Q, Yang W, Fu B, Pan Q (2021) A highly selective ratiometric fluorescent probe for doxycycline based on the sensitization effect of bovine serum albumin. J Hazard Mater 416:125759. https://doi.org/10.1016/j.jhazmat.2021.125759
35. Zhu H, Huang S, Ding M, Li Z, Li J, Wang S, Leong DT (2022) Sulfur defect-engineered biodegradable cobalt sulfide quantum dot-driven photothermal and chemodynamic anticancer therapy. Acs Appl Mater Int 14(22):25183–25196. https://doi.org/10.1021/acsami.2c05170
36. Zhu H, Li Z, Ye E, Leong DT (2021) Oxygenic enrichment in hybrid ruthenium sulfide nanoclusters for an optimized photothermal effect. Acs Appl Mater Int 13(50):60351–60361. https://doi.org/10.1021/acsami.1c17608
37. Zhong K, Hao C, Liu H, Yang H, Sun R (2021) Synthesis of dual-emissive ratiometric probe of BSA-Au NCs and BSA-Cu NCs and their sensitive and selective detection of copper and mercury ions. J Photochem Photobiol A 408:113100. https://doi.org/10.1016/j.jphotochem.2020.113100
38. Xie J, Zheng Y, Ying JY (2009) Protein-directed synthesis of highly fluorescent gold nanoclusters. J Am Chem Soc 131(3):888–889. https://doi.org/10.1021/ja806804u
39. Yang J, Li Z, Jia Q (2019) Design of dual-emission fluorescence sensor based on Cu nanoclusters with solvent-dependent effects: visual detection of water via a smartphone. Sensors Actuators B Chem 297:126807. https://doi.org/10.1016/j.snb.2019.126807